Dynamic-local-field approximation for the quantum solids

Richard D. Etters*

Colorado State University, Fort Collins, Colorado 80521

Ronald L. Danilowicz

NASA Lewis Research Center, Cleveland, Ohio 44135

(Received 5 October 1973)

A local-molecular-field description for the ground-state properties of the quantum solids is presented. The dynamical behavior of atoms contributing to the local field, which acts on an arbitrary pair of test particles, is incorporated by decoupling the pair correlations between these field atoms. The energy, pressure, compressibility, single-particle-distribution function, and the root-mean-square atomic deviations about the equilibrium lattice sites are calculated for H_2, ^3He, and ^4He over the volume range $5 < V \leq 24.5$ cm^3/mole. The results are in close agreement with existing Monte Carlo calculations wherever comparisons are possible. At very high pressures the results agree with simplified descriptions which depend on negligible overlap of the system wave function between neighboring lattice sites.

I. INTRODUCTION

The quantum solids have been difficult to understand analytically because of their large zero-point motion. This motion invalidates standard semiclassical approaches and those quantum-mechanical calculations which do not account for the short-ranged pair correlations between atoms.

Perhaps the most reliable theoretical description of the ground-state properties of quantum solids are the Monte Carlo calculations of Hansen and co-workers[1,2] on helium and Bruce[3] on hydrogen. This method is a quantum-mechanical analog of the biased random-walk procedure described by Wood and Parker.[4] Classically, the bias is established by the Boltzmann-probability distribution; whereas, quantum mechanically, it is given by the absolute square of the ground-state wave function $|\Phi|^2$. A parametrized form is generally chosen for Φ and the parameters are determined variationally by minimizing the ground-state energy.

A form for the N-particle wave function which satisfies the gross requirements of the system is

$$\Phi(\vec{r}_i, \ldots, \vec{r}_N) = \prod_{i=1}^{N} \varphi(\vec{r}_i) \prod_{j<\kappa}^{N} f(r_{j\kappa}), \qquad (1)$$

where the $\varphi(\vec{r}_i) \equiv \varphi(\vec{r}_i - \vec{R}_i)$ are single-particle functions localized about the equilibrium lattice sites $\vec{R}_i$. They exhibit spatial order characteristic of the solid. The $\frac{1}{2}N(N-1)$ functions $f(r_{j\kappa})$ correlate the motion of all pairs of particles. The limiting behavior for $f(r)$ is $\lim_{r \to 0} f(r) = 0$, $\lim_{r \to \infty} f(r) = 1$. Hence, these functions lower the probability of finding two molecules close together and they have no effect at large separations.

Although there are a number of aspects of the Monte Carlo method which can lead to significant

error,[4] it is generally believed that this approach is fairly reliable. For this reason, the results of our approximate theory are closely compared with the Monte Carlo calculations. Of course, comparisons with experiment are also made but it is difficult to draw definite conclusions from this information. The difficulty is that the semiphenomenological interaction potential, incorporated into the calculation, is of uncertain quality.[5] As pointed out by Hansen[6] and others, small differences in presently acceptable descriptions of the helium pair potential, significantly alter calculated results.

An important objective of this work is to provide an approximate yet accurate description of quantum solids. The detailed nature of these approximations are expected to give insight into the systems dynamical character by pinpointing those particular aspects of the many-body behavior which must be accurately described and those which are of lesser importance.

II. MOLECULAR-FIELD DESCRIPTION

A. General development

The expectation value of the Hamiltonian for an N-particle system is

$$\langle H \rangle = \langle \Phi | \Phi \rangle^{-1} \langle \Phi | - \frac{\hbar^2}{2m} \sum_{i=1}^{N} \nabla_i^2 + \sum_{i<j} V(r_{ij}) | \Phi \rangle, \quad (2)$$

where $V(r)$ is the pair potential and $\langle \Phi | \Phi \rangle$ is the normalization integral. To facilitate comparisons with other work, $V(r)$ is represented by the Lennard-Jones (6-12) potential:

$$V(r) = 4\epsilon[(\sigma/r)^{12} - (\sigma/r)^6], \qquad (3)$$

where $\sigma = 2.556$ Å, $\epsilon = 10.22$ K for helium[7] and σ

$= 2.958$ Å, $\epsilon = 36.7$ K for molecular hydrogen.[8] The ground-state wave function Φ is given by Eq. (1), where

$$\varphi(\vec{r}_i) = (\beta/\pi)^{3/4} e^{-(\beta/2)(\vec{r}_i - \vec{R}_i)^2}, \tag{4}$$

$$f(r) = e^{-(\kappa/r)^{5/2}}. \tag{5}$$

The quantities β and κ are variational parameters to be determined. These forms for φ and f are used extensively in other related works where they appear to have sufficient flexibility to adequately represent the ground state of the system.[1-3] They are also adopted here partially because of the stated objective to compare this approximate theory with other calculations.

Using Green's theorem and with Eqs. (1), (4), and (5), Eq. (2) becomes

$$\langle H \rangle = \frac{3N\hbar^2\beta}{4m} + \langle \Phi | \Phi \rangle^{-1} \sum_{i<j} \int \Phi^2 v(r_{ij}) d\vec{r}_1 \cdots d\vec{r}_N, \tag{6}$$

where

$$v(r_{ij}) = V(r_{ij}) - (\hbar^2/2m)\nabla_i^2 \ln f(r_{ij}). \tag{7}$$

For the purposes of this calculation, it is convenient to rewrite Eq. (6) in the following form:

$$\langle H \rangle = \frac{3N\hbar^2\beta}{4m} + \langle \Phi | \Phi \rangle^{-1} \sum_{\lambda < \kappa}^{N} \int \varphi^2(\vec{r}_\lambda)\varphi^2(\vec{r}_\kappa)$$

$$\times f^2(\vec{r}_{\lambda\kappa}) v(\vec{r}_{\lambda\kappa}) G(\vec{r}_\lambda, \vec{r}_\kappa) d\vec{r}_\lambda d\vec{r}_\kappa, \tag{8}$$

where

$$G(\vec{r}_\lambda, \vec{r}_\kappa) = \int \prod_{i<j \neq (\lambda,\kappa)}^{N} f^2(\vec{r}_{ij})$$

$$\times \prod_{s \neq \lambda,\kappa}^{N} |\varphi(\vec{r}_s)|^2 d\vec{r}_1 \cdots (d\vec{r}_\lambda d\vec{r}_\kappa)^{-1} \cdots d\vec{r}_N. \tag{9}$$

The parentheses around the term $(d\vec{r}_\lambda d\vec{r}_\kappa)^{-1}$ indicate that integrals over the enclosed variables are deleted. At this point the calculation is exact and it is here that different theoretical descriptions diverge. An examination of Eq. (9) shows that each particle in the system is dynamically coupled to every other particle through the pair-correlation functions $f(r_{ij})$. It is therefore obvious that a drastic approximation is necessary to reduce this coupled N-body problem to a tractable form.

In the Nosanow cluster-expansion approximation,[9] evaluated to second order, the approximation is very drastic. It is assumed that $G(\vec{r}_\lambda, \vec{r}_\kappa) \simeq 1$. The supporting argument is that the $f(r)$ in Eq. (9) have already reached their asymptotic values of unity for values of $\vec{r}$ where the integrand in Eq. (8) is large. Under these conditions, the volume in-

tegration of $\Pi_s |\varphi(r_s)|^2$ terms in Eq. (9) give unity. This was the first approximate calculation to yield reasonable results for solid helium even though, by present standards, the results are not very good. A serious flaw in the cluster expansion as an ultimate theoretical description was pointed out by Guyer.[10] He showed that the only possible wavefunction resulting from an internally self-consistent solution was a nonlocalized liquid-state function.

In view of the deficiencies in the cluster-expansion method and other approximate theories, it is apparent that the behavior of each molecule depends strongly on the influence of large numbers of neighboring molecules. Equations (8) and (9) show that the effect of all N-2 other molecules on an arbitrary dynamical pair, hereafter labeled (λ, κ), is embodied in $G(\vec{r}_\lambda, \vec{r}_\kappa)$. The work presented in this article is directed at accounting for this local molecular field acting on each pair (λ, κ) and produced by the presence of the N-2 other molecules. The major approximation underlying this calculation is contained in the expression

$$G(\vec{r}_\lambda, \vec{r}_\kappa) \simeq \prod_{s \neq \lambda, \kappa}^{N} \int [f^2(r_{\lambda s}) f^2(r_{\kappa s})\varphi^2(\vec{r}_s - \vec{R}_s) d\vec{r}_s]. \tag{10}$$

This expression for $G(\vec{r}_\lambda, \vec{r}_\kappa)$ differs from Eq. (9) in that it contains no direct correlations between the N-2 atoms comprising the molecular field which acts on (λ, κ). That is, the $f(r_{ij})$ which connect molecular-field atoms to one another are missing in Eq. (10). Only those pair correlations which directly link the N-2 atoms of the molecular field to the dynamical pair (λ, κ) are considered. This approximation is essential in that it simplifies the problem to the extent that a tractable solution is possible which still preserves the important features of the system's behavior.

B. Static-field approximation

The lowest-order approximation which takes into account the local field acting on a pair (λ, κ), due to the N-2 other molecules, is a static field. That is, all N-2 contributing molecules are fixed at their equilibrium lattice sites. This is operationally accomplished by taking the limit

$$\lim_{\beta \to \infty} |\varphi(\vec{r}_i - \vec{R}_i)|^2 - \delta(\vec{r}_i - \vec{R}_i)$$

for all $i \neq \lambda, \kappa$ in Eq. (9). Then

$$G(\vec{r}_\lambda, \vec{r}_\kappa) = \prod_{i \neq \lambda, \kappa}^{N} f^2(\vec{r}_\lambda - \vec{R}_i) \prod_{j \neq \lambda, \kappa}^{N} f^2(\vec{r}_\kappa - \vec{R}_j). \tag{11}$$

In an earlier work[11] this expression was further simplified by limiting the products over (i, j) to

include only nearest neighbors of molecules (λ, κ). Then each function $f^2(\vec{r}_\lambda - \vec{R}_i)$ was expanded about its value evaluated at the equilibrium lattice site $\vec{r}_\lambda = \vec{R}_\lambda$, and angle averaged. This procedure was similarly applied to the $f^2(\vec{r}_\kappa - \vec{R}_j)$. The expectation value of the Hamiltonian [Eq. (8)] then reduced to an easily soluble two-dimensional integral. Although the results were fairly promising, it was later established that the expansion of the $f(r)$ about their equilibrium lattice positions converge satisfactorily only for a limited class of pair correlation functions, namely those which reach their asymptotic values for values of $r \lesssim R_0$, where R_0 is the equilibrium nearest-neighbor separation. This limited variational capability was considered unsatisfactory and the procedure was therefore abandoned.

A more direct approach, hereafter called the "static-field" approximation, is to evaluate Eq. (11) exactly but only for a limited number of correlations. In bcc solid helium, for example, only pair correlations between atoms within three nearest-neighbor shells of atom λ have any appreciable effect on the behavior of the λth atom and similarly for the κth atom. All the other $f(r)$ in Eq. (11) can be replaced by unity with the effect of changing predicted ground-state energies by less than 1%. For fcc molecular hydrogen, two nearest-neighbor shells are sufficient to produce equivalent accuracy. The $G(\vec{r}_\lambda, \vec{r}_\kappa)$ resulting from this procedure was substituted into Eq. (8) and the lattice sum was evaluated for all different (λ, κ) pairs up to tenth nearest neighbors. Beyond that, lattice sums were evaluated for a classical static lattice. The error associated with this lattter procedure is extremely small, on the order of 0.1%. The six-dimensional integrals in Eq. (8) were evaluated on a 7094 computer. Although the results are reasonably good at low pressures, their agreement with experiment becomes considerably worse as the pressure increases. Another disquieting feature of the calculation is that the minimum energy is obtained at all volumes for a value of the parameter $\beta = 0$. The energy actually varies quite slowly with β for small β. In the cluster expansion, $\beta = 0$ implies that the solid is not stable because the functions $\varphi(r)$ in Eq. (1) are no longer spatially localized. This difficulty does not exist in the static-field approximation because $G(\vec{r}_\lambda, \vec{r}_\kappa)$, rather than being unity as in the cluster expansion, is instead given by Eq. (11). The resulting internal field, acting on (λ, κ) produce the restoring force necessary to localize the atoms about their equilibrium lattice sites $\{R_i\}$. This localization is evident upon calculating the single-particle distribution function $R(r)$, in terms of the atomic displacement from equilibrium, $r = |\vec{r}_i - \vec{R}_i|$. These

data are presented in Sec. IIIA. Nevertheless, the static-field approximation is, in some sense, internally inconsistent. On one hand the molecular-field atoms are initially fixed on their equilibrium lattice sites by taking the limit $\beta \to \infty$, yet the minimization of the energy gives the result $\beta = 0$ for the test particles (λ, κ).

C. Dynamic-field approximation

It is believed that the lack of good agreement between the static field results and experiment is due primarily to the rigidity of the lattice producing the local molecular field on (λ, κ). As an example, when an excursion of particle λ takes it into close proximity to molecular-field atom j, the molecular-field atom will tend to move out of the way. This cannot happen in the static-field approximation. The motion of (λ, κ) is, therefore, restricted. In order to correct this deficiency in the theory, the motion of nearest neighbors to molecules λ and κ has been incorporated into the calculation of the molecular field. Then

$$G(\vec{r}_\lambda, \vec{r}_\kappa) = \prod_{s \neq nn\lambda}{}' f^2(r_\lambda - R_s) \prod_{\rho \neq nn\kappa}{}' f^2(r_\kappa - R_\rho)$$

$$\times \prod_{i=nn\lambda}{}' M_i(\vec{r}_\lambda) \prod_{j=nn\kappa}{}' M_j(\vec{r}_\kappa)$$

$$\times \prod_{l=nn\lambda\kappa}{}' N_l(\vec{r}_\lambda, \vec{r}_\kappa), \tag{12}$$

where the primes indicate that the product is not to include index λ or κ, $nn\lambda$ — nearest neighbors to particle λ, $nn\lambda\kappa$ — nearest neighbors to particles λ and κ.

$$M_j(\vec{r}_\kappa) = \int f^2(r_{\kappa j})\varphi^2(\vec{r}_j - \vec{R}_j)\, d\vec{r}_j, \tag{13}$$

$$N_l(r_\lambda, r_\kappa) = \int f^2(r_{\lambda l})f^2(r_{\kappa l})\varphi^2(\vec{r}_l - \vec{R}_l)\, d\vec{r}_l. \tag{14}$$

The first two products in Eq. (12) include all atoms which are second- or third-nearest neighbors to λ or κ. These products are simply the static-field terms. As in the static-field approximation, pair correlations beyond third-nearest neighbors are neglected, a procedure which leads to no appreciable error. The third product in Eq. (12) extends over all nearest neighbors to λ except for κ. As an example, consider a bcc lattice with (λ, κ) nearest neighbors. Then there are seven terms in that product. The fourth product in Eq. (12) is, of course, similar to the third. The last product does not exist in this case because there are no nearest neighbors common to both λ and κ when they themselves are nearest neighbors. When λ

and κ are second-nearest neighbors, however, there are four atoms which are nearest neighbors to both λ and κ. Then, the last three products in Eq. (12) each contain four terms. Slightly different results are, of course, obtained for fcc and hcp structures. When λ and κ are third-nearest neighbors or greater we simply return to the static-field approximation, in which case

$$M_j(\vec{r}_\kappa) \simeq f^2(\vec{r}_\kappa - \vec{R}_j),$$
$$N_i(\vec{r}_\lambda, \vec{r}_\kappa) \simeq f^2(\vec{r}_\lambda - \vec{R}_i) f^2(\vec{r}_\kappa - \vec{R}_i). \qquad (15)$$

Again, for (λ, κ) separated farther than tenth-nearest neighbors, the lattice sums are simply taken over a static lattice. Clearly, it is the integrals N and M in Eq. (12) which provide the dynamical correlations connecting atoms (λ, κ) to the local field. Although the atoms responsible for the local field couple dynamically to atoms λ and κ, they do not couple dynamically to one another, as evidenced by the separable integrals in Eq. (12). The reason for this fortunate circumstance is, of course, traced to the original approximation, exhibited in Eq. (10). This separability reduced an impossibly complex analysis to that of evaluating a simple nine-dimensional integral on the 7094 computer. The details of this procedure are discussed in the Appendix.

To summarize, the dynamical motion of the molecular-field atoms and the effect of this motion on the various pairs (λ, κ) considered only when λ and κ are either first- or second-nearest neighbors to one another. Then only molecular-field atoms which are nearest neighbors to λ and/or κ are dynamically incorporated into the analysis. All other pair correlations are with a static field. It is clear that the dynamical correlations have been incorporated only into the leading terms in the
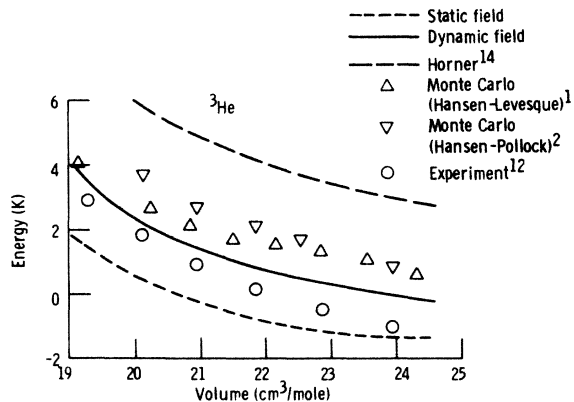
lattice sum, that is, for all first- and second-nearest-neighbor pairs. Nevertheless, this is sufficient to dramatically improve the results. Additional dynamical contributions are found to be small.

Within the dynamic-field approximation, the single-particle distribution function $R(r)$ is simply

$$R(|\vec{r}_\lambda - \vec{R}_\lambda|) = \int \varphi^2(\vec{r}_\lambda - \vec{R}_\lambda)\varphi^2(\vec{r}_\kappa - \vec{R}_\kappa) f^2(r_{\lambda\kappa})$$
$$\times G(\vec{r}_\lambda, \vec{r}_\kappa) d\vec{r}_\kappa \, d\Omega_\lambda, \qquad (16)$$

where $d\Omega_\lambda$ is the element of solid angle for the λth particle, $G(\vec{r}_\kappa, \vec{r}_\lambda)$ is given by Eq. (11), and the normalization $R(0) = 1.0$ is used. A similar expression as Eq. (16) exists for the root-mean-square atomic deviation from its equilibrium lattice site $\langle r^2 \rangle^{1/2}$. The pressures and compressibilities are derived by taking appropriate derivatives of the ground-state energy with respect to the volume.

III. RESULTS AND DISCUSSION

A. Static-field approximation

Results for the ground-state energy of solid bcc ^{3}He and ^{4}He are presented on Figs. 1 and 2. We are not concerned with the fact that solid helium also exists in a close-packed lattice phase because the energy difference between different structures are known to be very small. In these figures, the circles represent the experimental data[12] and the dotted line represents the results of the static-field approximation. The triangles represent the Monte Carlo (MC) calculation of Hansen and Levesque[1] and the inverted triangles represent a similar MC calculation by Hansen and Pollock.[2] Although the static-field results compare reason-

FIG. 1. Energy vs volume for solid bcc ^{3}He. A comparison is made with different theoretical and experimental works.
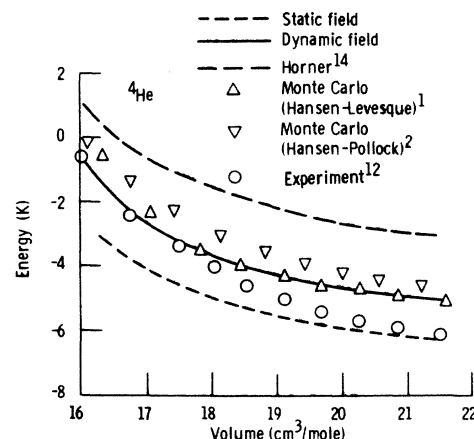

FIG. 2. Energy vs volume for solid ^{4}He. A comparison is made with different theoretical and experimental works.
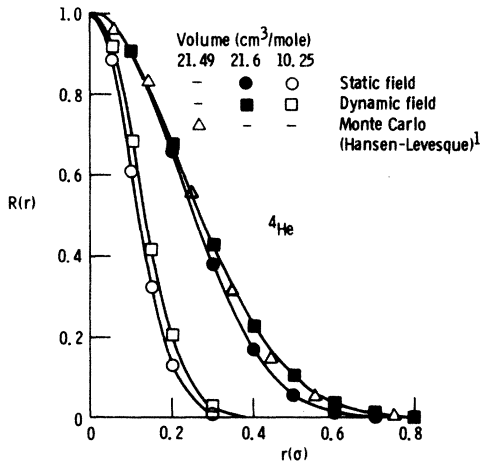
FIG. 3. Single-particle distribution function $R(r)$ for solid ^{4}He at two different volumes, as a function of the particle displacement from equilibrium r. The results of two different approximation methods are compared to one another and also to results from a Monte Carlo calculation.

ably well with experiment and with the MC results in the volume range shown, the comparison becomes increasingly unfavorable as the molar volume is decreased.

The single-particle-distribution function $R(r)$ for ^{4}He, at several different volumes, is shown on Fig. 3 as a function of the particle displacement from equilibrium $r = |\vec{r}_i - \vec{R}_i|$. The circles represent the results of the static-field approximation, from which it is evident that the atoms remain localized despite the fact that $\beta = 0$ minimizes the energy. These results are compared with the MC results of Hansen and Levesque,[1] which are represented by the triangles. The values of κ which minimize the energy in the static-field approximation are larger than those derived from MC calculations.[1,2] This is understandable because, with $\beta = 0$, the various $f(\vec{r}_\kappa - \vec{R}_i)$ are entirely responsible for providing the localization necessitating a larger κ value.

As mentioned earlier, it is believed that the results of the static-field approximation are not

totally satisfactory because of the rigidity of the lattice of atoms providing the local field. The dynamical motion of an arbitrary atom λ is inhibited because the fixed atoms confine λ to a smaller effective volume than it would have if the atoms producing the local field were allowed to move in response to the motion. This situation apparently becomes more critical at higher pressure where the effective volume per atom is further reduced. McMahan[13] has recently calculated the exchange integral J for solid ^{3}He by an approach that is apparently very similar to the static-field method. Although his results are reasonable at low pressure, they become increasingly unfavorable as the pressure increases. McMahan concludes as we do that the rigidity of the lattice is to blame and that this effect is more pronounced at higher densities.

The solution then is to properly describe the motion of the molecular-field atoms and the effect of this motion on all dynamical pairs (λ, κ). The results of this dynamic-field approximation are now described.

B. Dynamic-field approximation

1. ^{3}He data

Results for solid ^{3}He are presented in Table I, where $\langle T \rangle$ and $\langle V \rangle$ are the expectation values of the kinetic and potential energies, respectively, and E_0 is the total ground-state energy. The quantities β and κ are values of the variational parameters which minimize the energy and $\langle r^2 \rangle^{1/2}$ is the root-mean-square atomic deviation from the equilibrium lattice site. Pressures and compressibilities are also tabulated. It should be kept in mind that all work on helium was done using a bcc lattice structure. Although the total energy, pressure, and compressibility do not differ significantly from one assumed lattice structure to another, the quantities $\langle T \rangle$, $\langle V \rangle$, and $\langle r^2 \rangle^{1/2}$ are somewhat more sensitive and any comparisons with other work must be made with this fact in mind.

Figure 1 shows the ground-state energy for ^{3}He over the volume range $19 \leqslant V \leqslant 24.5$ cm^3/mole. The

TABLE I. bcc ^{3}He results.

Volume (cm^3/mole)	$\langle V \rangle$ (K)	$\langle T \rangle$ (K)	E_0 (K)	Pressure (atm)	Compressibility (10^4 atm^{-1})	$\langle r^2 \rangle^{1/2}$ A	β (σ^{-2})	κ (σ^{-1})
24.50	−22.19	21.94	−0.25			1.18	3.6	1.11
20.80	−26.98	28.38	1.40	50	23.8	1.06	4.1	1.11
16.16	−32.31	41.12	8.81	260	7.0	0.85	6.5	1.08
14.00	−32.21	51.43	19.22	565	3.9	0.75	8.7	1.06
11.82	−24.76	69.70	44.94	1380	1.8	0.62	12.5	1.04
10.25	−8.30	92.25	83.95	2820	0.7	0.52	19.0	1.02

circles represent experimental data,[12] the triangles are the MC results of Hansen and Levesque,[1] and the inverted triangles are the MC results of Hansen and Pollock.[2] The solid line represents the dynamic-field results, the dotted line is the static-field results, and the dashed line represents the theory of Horner.[14] A sample comparison of our calculated energy and that of Hansen and Levesque at $V = 24.3$ cm^3/mole is $E = 0.21$ and 0.63 K, respectively. Similarly, at $V = 19.12$ cm^3/mole, the comparison is $E = 4.01$ and 4.07 K, respectively. It is interesting to observe that results of the two MC calculations differ from one another by amounts that are significantly outside the statistical error quoted in either article. There are, however, modest differences in the two calculations which could account for this fluctuation. The dynamic-field approximation requires the evaluation of a nine-dimensional integral. These integrals have been evaluated with sufficient accuracy to conservatively guarantee the resulting energy values to within ~3%. In view of the fluctuation in the MC results we conclude that they and the dynamic-field results are in agreement. The energy minimizing values for β and κ, listed in Table I, also compare well with the MC results, unlike the values derived from the static-field approximation. Figure 4 shows the ground-state energy over a greater volume range $10 < V \leq 24.5$ cm^3/mole. A sample comparison of our calculated energy with that of Hansen and Pollock at $V = 11.17$ cm^3/mole gives $E = 54.17$ and 52.5 K, respectively. We observe, as do Hansen and Pollock, that the energy falls below the experimental values at low volumes. This is attributed to the inexact description of the pair interaction provided by the Lennard-Jones 6-12 potential.[5] Figure 5 shows the pressure-volume (PV) relationship and, in Fig. 6, is the single-particle distribution function $R(r)$ for six different volumes. These data are tabulated in Tables I and II. The compressibility is shown in Fig. 7 and compared with experiment over the
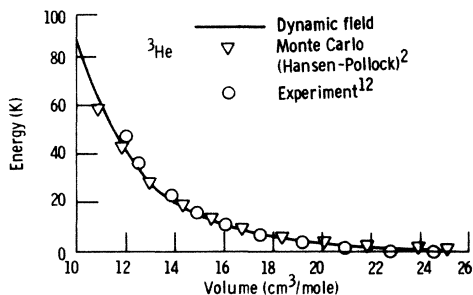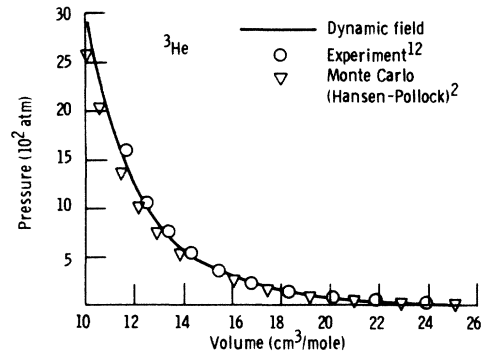
FIG. 5. Pressure vs volume for solid ^{3}He. A comparison is made with other theoretical work and experiment.

volume range $10 \leq V \leq 24.5$ cm^3/mole. These results are substantially more uncertain than the energy because they involve a second derivative of the energy with respect to the volume.

2. ^{4}He results

The calculated data for solid ^{4}He are presented in Table III. Figure 2 shows the ground-state energy over the volume range $16 \leq V \leq 21.65$ cm^3/mole. Similarly, Fig. 8 shows the energy over a greater volume range $10 \leq V \leq 21.65$ cm^3/mole. The experimental data[12] and other theoretical results are presented with the same format as Figs. 1 and 4 for ^{3}He. A sample comparison of our calculated energy and that of Hansen and Levesque at $V = 21.49$ cm^3/mole is $E = -5.14$ and -5.17 K, respectively. Similarly, at $V = 17.08$ cm^3/mole, the comparison is $E = -2.63$ and -2.39 K, respectively. A comparison with Hansen and Pollock's

FIG. 4. Energy vs volume for solid ^{3}He over the volume range $10 < V \leq 24.5$ cm^3/mole. A comparison is made with other theoretical work and experiment.
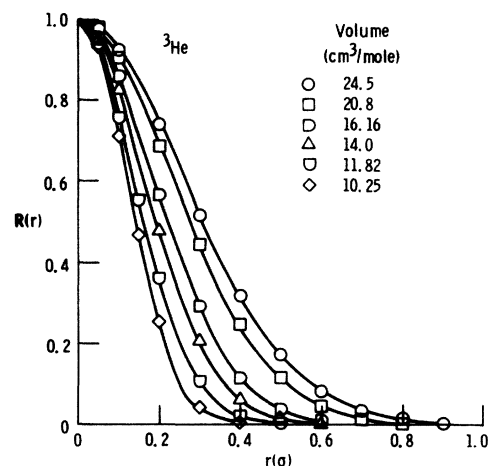
FIG. 6. Single-particle distribution function $R(r)$ vs particle displacement from equilibrium for solid ^{3}He at various volumes.

TABLE II. $R(r)$ data for ^{3}He.

Volume (cm^3/mole)	0	0.05	0.10	0.15	0.20	0.30	0.40	0.50	0.60	0.70	0.80
10.25	1.00	0.928	0.717	0.466	0.254	0.042	0.0035				
11.82	1.00	0.935	0.757	0.559	0.363	0.107	0.019	0.0018			
14.00	1.00	0.957	0.824		0.480	0.206	0.060	0.012	0.0015		
16.16	1.00	0.961	0.859		0.567	0.293	0.117	0.036	0.0078		
20.8	1.00	0.975	0.905		0.688	0.445	0.246	0.116	0.046	0.0148	0.0039
24.5	1.00		0.922		0.738	0.515	0.317	0.173	0.083	0.034	0.012

work at $V = 11.17$ cm^3/mole gives $E = 32.06$ and 30.15 K, respectively. Again, it is evident that there is close agreement between experiment, the MC calculation, and the dynamic-field results. As for ^{3}He, however, calculated results lie slightly below experiment at the higher pressures. Figure 9 shows the PV results and Figs. 3 and 10 give the single-particle distribution function for solid ^{4}He for various molar volumes. Note the considerable narrowing of $R(r)$ with decreasing molar volume. Figure 3 shows a comparison of results for $R(r)$ at $V = 21.6$ cm^3/mole obtained from the static-field approximation and from the dynamic-field approximation. As expected, the static-field approximation yields a narrower $R(r)$ indicating that the particle is more localized about its equilibrium lattice site than is predicted by the dynamic-field approximation. This result, of course, confirms our speculation that the static molecular field confines λ and κ more than if the molecular-field atoms also are allowed to dynamically respond to a changing environment, as provided for in the dynamic-field approximation. Also shown in Fig. 3 is the MC solution[1] for $R(r)$. The close comparison with the dynamic-field approximation is evident. The data for $R(r)$ is tabulated in Table IV.

3. Molecular-hydrogen results

In Fig. 11 the energy of molecular hydrogen is presented over the volume range $10 \leqslant V \leqslant 22.65$
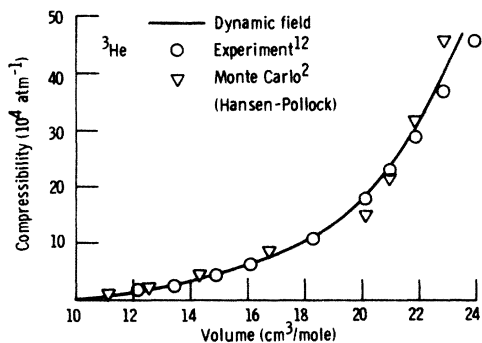
FIG. 7. Compressibility vs volume for solid ^{3}He.

cm^3/mole. All calculations on H_2 are based on an fcc lattice structure. The solid line represents the results of the dynamic-field approximation and the squares show the MC calculations of Bruce.[3] The triangles display the Heitler-London results of Etters, Raich, and Chand[15] and the inverted triangles represent a Domb-Salter[16] approximation scheme. At normal vapor pressure, $V = 22.65$ cm^3/mole, the dynamic-field calculation gives a ground-state energy $E_0 = -85$ K, which is virtually identical to the MC result of Bruce. At $V = 11.39$ cm^3/mole, a comparison of our work with Bruce's gives $E = 444.71$ and 445.34 K, respectively. Similarly, at $V = 8.34$ cm^3/mole, the comparison is $E = 2296.51$ and 2300.83 K, respectively. The dynamic-field and the MC results agree closely over the entire volume range, but not with the Heitler-London[15] and Domb-Salter[16] calculation, especially at the lower densities. This is not surprising since the latter two calculations are inherently unreliable at low pressure. In Fig. 12, the energy is displayed for the volume range $5 \leqslant V \leqslant 11$ cm^3/mole. The comparisons and format are identical to Fig. 11. It is apparent that, at these high pressures, the results of all four calculations displayed here are in fair agreement with one another. However, the MC data of Bruce extends only to $V = 9.34$ cm^3/mole. The pressure-volume data is shown in Fig. 13 for the volume range $10 \leqslant V \leqslant 22.65$ cm^3/mole. In addition to the format of Figs. 11 and 12, the experimental data of Stewart[17] are displayed as circles. It is apparent that, at low molar volumes, the different theoretical calculations all predict pressures considerably higher than experiment.[17] Until recently, it was considered possible that this discrepancy was due to experimental effects. However, recent measurements indicate that the original data was reasonably accurate.[18] It also appears certain that the theoretical calculations are fairly accurate at high densities.[15] Hence, the discrepancy between theory and experiment is almost certainly due to the poor representation of the pair interaction provided by the Lennard-Jones 6-12 potential. In Fig. 14 the pressure calculated over the volume range $5 \leqslant V \leqslant 11$ cm^3/mole is

TABLE III. bcc ^{4}He results.

Volume (cm^3/mole)	$\langle V \rangle$ (K)	$\langle T \rangle$ (K)	E_0 (K)	Pressure (atm)	$\langle r^2 \rangle^{1/2}$ (A)	β (σ^{-2})	κ (σ^{-1})
21.60	−27.48	22.29	−5.19		1.03	4.5	1.13
17.50	−34.27	30.85	−3.42	93	0.83	5.7	1.13
15.50	−38.9	39	0.1	250	0.76	8.0	1.12
13.75	−40.46	49.07	8.61	500	0.64	11.5	1.11
11.82	−40.46	65.83	25.37	1035	0.56	15.0	1.10
10.25	−31.25	83.42	52.17	1790	0.48	20.0	1.10

presented. The close agreement of the dynamic-field results to those derived from the Heitler-London[15] and Domb-Salter[16] calculations indicates that the overlap of the wave function between neighboring sites is very small at these pressures. Otherwise, these latter two approximate methods would not yield satisfactory results. The results confirm the claim[15, 16] that solids become more and more classical in behavior as the pressure is increased. The data for H_2 are tabulated in Table V.

IV. CONCLUSIONS AND DISCUSSION OF APPROXIMATIONS

There are two features of the Monte Carlo calculations that make them suspect at high pressures. At high enough pressures, the number of atoms contained in a volume sufficiently large to simulate the bulk system becomes great, perhaps beyond available computer resources. Then any proposed solution requires a compromise which weakens the integrity of the results. In addition, the Monte Carlo program may not sample phase

space ergodically at high pressure because the close-packed repulsive potential cores give rise to walls of very low probability surrounding regions of high probability. This difficulty has been well documented for a collection of hard disks.[4] We have been concerned that the poor agreement at high pressures between the MC results for helium and experiment is from one of these effects. The close comparisons between the dynamic-field calculations and the MC work[1, 2] dispell that concern, however, because the dynamic-field approximation is in no way limited at high pressures. In addition, the unsatisfactory nature of the Lennard-Jones 6-12 potential at high pressure has also been demonstrated by others, using a simplified theoretical approach.[5]

The variational parameter κ, which minimizes the energy, remains essentially constant at all volumes for both helium and hydrogen. For molecular hydrogen this parameter remains very near $\kappa \approx 1.13$ over the entire volume range $5 \leqslant V \leqslant 22.65$ cm^3/mole. This general result agrees completely with the findings of Hansen and Pollock on helium[2] but not quite so well with those of Bruce on hydrogen.[3] The results of Bruce are admittedly not calculated to high accuracy and it is our opinion that κ is approximately density independent. We agree with Hansen and Pollock that
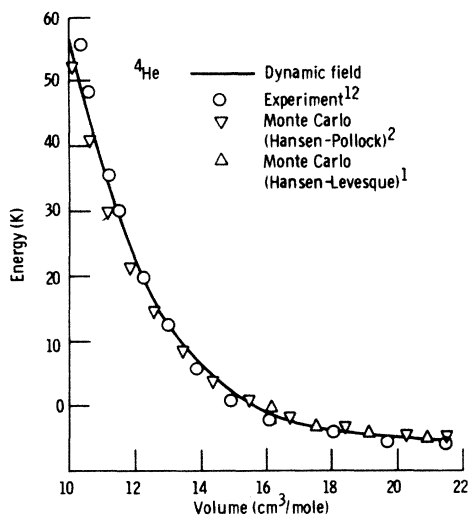

FIG. 8. Energy vs volume for solid ^{4}He over the volume range $10 \leq V \leq 21.65$ cm^3/mole. A comparison is made with other theoretical work and experiment.
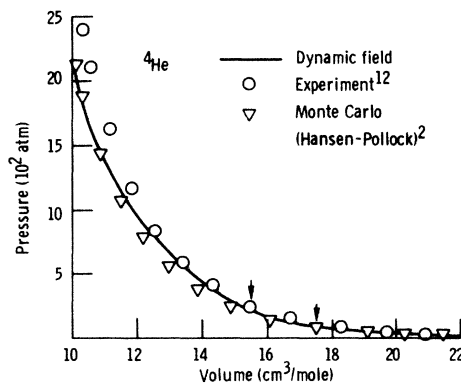

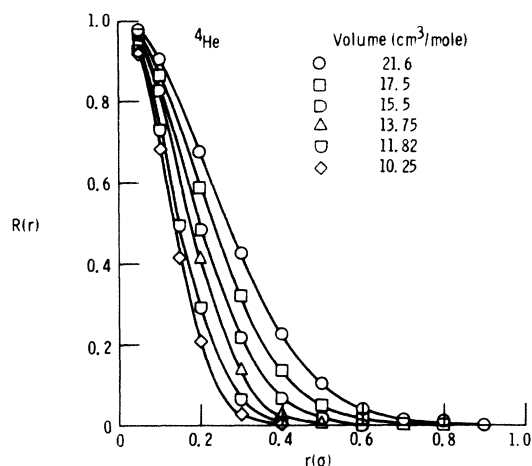FIG. 9. Pressure vs volume for solid ^{4}He. A comparison is made with other theoretical work and experiment.

FIG. 10. Single-particle distribution function $R(r)$ vs particle displacement from equilibrium for solid ^{4}He at various volumes.

this result illustrates the importance of pair correlations at all pressures but it is worth emphasizing that approximate approaches such as the Heitler-London method and the Domb-Salter approximation also properly account for these correlations at high pressures. With increasing density, the dependence of the energy upon the parameter β becomes increasingly weak. That is, the energy minimum with respect to β forms a very shallow well. Hydrogen, for example, has an energy minimum at 9 cm^3/mole for $\beta \approx 150$. However, for $\beta = 100$, the energy is less than 1% greater than the minimum value. The physical implications of this result are not fully understood. Because of this relatively weak dependence of the energy on β, the minimizing values of β listed in the tables are not very accurate at the higher pressures.

An important approximation in the dynamic-field method is the cutoff of products of two-body-correlation functions $f(r_{ij})$. The products retained in

$G(\vec{r}_\lambda, \vec{r}_\kappa)$ are the correlations of molecules λ and κ to their first-, second-, and third-nearest neighbors. The functions f outside this range are replaced by unity. Some idea of the effect of this approximation can be seen in Table VI where $\langle T \rangle$, $\langle V \rangle$, and E_0 are presented for a typical ^{4}He calculation of 21.6 cm^3/mole. These results are displayed as a function of the number of nearest-neighbor shells contained in the product of pair-correlation functions $f(r_{ij})$. As can be seen from the table, these results converge quickly even though the $f(r)$ used in this study are fairly long ranged. Most of the results for H_2 were obtained with a second-nearest-neighbor cutoff in products of $f(r)$, a procedure which resulted in negligible error.

As mentioned earlier, the integrals in the lattice sum of Eq. (8) were calculated exactly only for the first ten nearest-neighbor shells. The contributions from remaining shells are evaluated for a static lattice. It was found that over the range of densities studied, the energy could be determined to within 0.5 K if only the contributions from the first four nearest-neighbor shells were calculated exactly, with the other shells being evaluated for a static lattice. This approximation is made in most Monte Carlo studies.[1-3] The use of static lattice sums after ten nearest-neighbor shells leads to negligible error. Some idea of the magnitude of contributions to the energy from different nearest-neighbor shells can be seen in Table VII. This table contains contributions to $\langle T \rangle$, $\langle V \rangle$, and E_0 from different groups of nearest-neighbor shells for ^{4}He at 21.6 and 10.25 cm^3/mole. As can be seen from this table, the contributions from the first two nearest-neighbor shells are very large at low density. The contributions from other shells become increasingly important with higher densities. However, the contributions from the first four or five shells dominate the total energy even at these high densities.

TABLE IV. $R(r)$ data for He^4

| Volume (cm^3/mole)	Particle displacement from equilibrium $r(\sigma)$										
	0.0	0.05	0.10	0.15	0.20	0.30	0.40	0.50	0.60	0.70	0.80
10.25	1.00	0.916	0.681	0.417	0.207	0.027	0.0012				
11.82	1.00	0.922	0.730	0.495	0.292	0.064	0.0070				
13.75	1.00	0.955	0.809		0.412	0.133	0.026	0.0028			
15.50	1.00		0.829		0.484	0.217	0.068	0.019	0.0022	0.0019	
17.50	1.00		0.862		0.587	0.319	0.137	0.045	0.011	0.011	0.0028
21.60	1.00		0.901		0.675	0.424	0.227	0.102	0.038		
					Static-field approximation						
10.25	1.00	0.885	0.610	0.323	0.130	0.0084	0.00015				
21.60	1.00	0.975	0.902		0.657	0.380	0.168	0.054	0.013	0.0022	0.00032
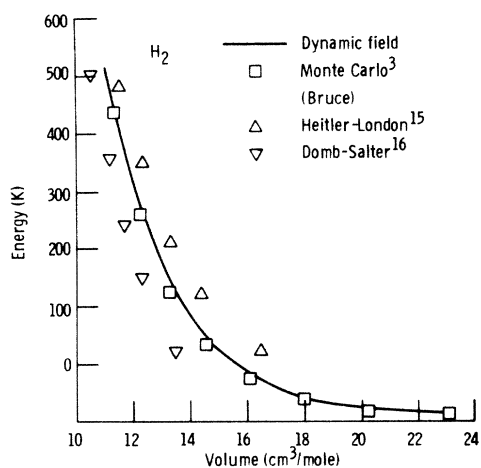
FIG. 11. Energy vs volume for solid fcc H_2 over the volume range $10 \le V \le 22.65$ cm^3/mole. A comparison is made with other theoretical work.

Figure 15 contains a comparison of the single-particle distribution function and $e^{-\beta r^2}$ for ^{4}He at two specific volumes. The quantity $e^{-\beta r^2}$ would be the single-particle distribution function if the wave function did not contain pair correlations. This figure, therefore, gives some indication of how much the pair correlations contribute to localizing the individual molecules about their equilibrium lattice sites. Note that the pair-correlation functions are responsible for a substantial portion of
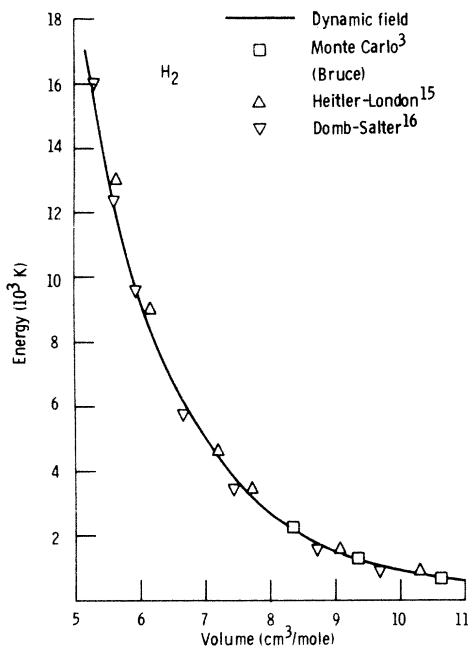

FIG. 12. Energy vs volume for solid fcc H_2 over the volume range $5 \le V \le 11$ cm^3/mole. A comparison is made with other theoretical work.

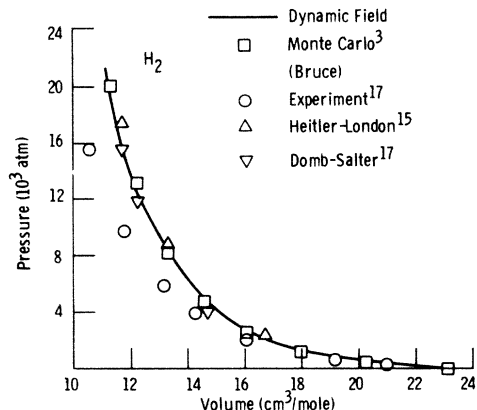

FIG. 13. Pressure vs volume for solid fcc H_2 over the volume range $10 \le V \le 22.65$ cm^3/mole. A comparison is made with other theoretical work and experiment.

the localization at both volumes tested.

To recapitulate, the principal approximation of this calculation is the decoupling of pair correlations between different molecular-field atoms, as exhibited by Eq. (10). This approximation together with the others already discussed earlier in this section, have lead to a theoretical description of solid ^{3}He, ^{4}He, and H_2 which is essentially in very close agreement with the results of Monte Carlo calculations. The agreement with experiment is also excellent, except at high pressures, where, for both helium and hydrogen, the poor comparisons are attributed to an inadequate representation of the pair potential.

Several major advantages over the Monte Carlo work accrue to this method of calculation. In addition to the considerably less computational effort required and the physical insight afforded by the the successful approximation techniques,
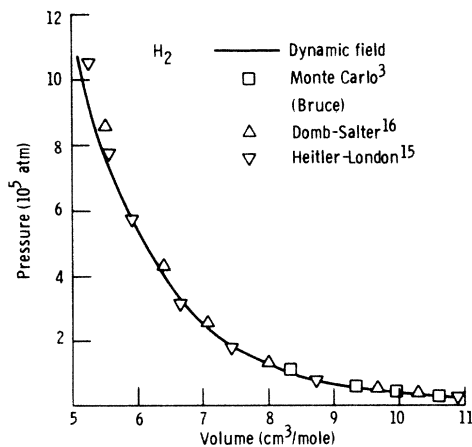

FIG. 14. Pressure vs volume for solid fcc H_2 over the volume range $5 \le V \le 11$ cm^3/mole. A comparison with other theoretical work is made.

TABLE V. Results.

Volume (cm³/mole)	$\langle V \rangle$ (K)	$\langle T \rangle$ (K)	E_0 (K)	Pressure (atm × 10³)	β (σ^{-2})	κ (σ^{-1})
23.30	−150.5	65.5	−85.0		7	1.19
18.52	−188.0	126.0	−62.0	1.06	30	1.14
13.99	−149.0	243.5	94.5	6.12	67	1.12
12.35	− 25.5	297.5	272.0	11.95	80	1.11
11.11	159.0	353.5	512.5	21.69	95	1.10
9.26			1306	60.1	150	1.12
7.72			3120	147.7	300	1.10
6.17			8290	454.9	375	1.10
5.56			12 280	726.0	500	1.12
5.14			17 000	998.0	650	1.12

it is in principal possible to determine and solve the coupled differential equations for the optional form of φ and f which minimize the energy. This is possible because the dynamics of only a limited number of particles are involved. Another valuable feature is that the exchange energy can be calculated in a simple direct fashion. Work on this problem is in progress.

APPENDIX

To evaluate $G(\vec{r}_\lambda, \vec{r}_\kappa)$ for a particular value of $\vec{r}_\lambda$ and $\vec{r}_\kappa$, there are a product of three-dimensional integrals to solve, i.e.,

$$G(\vec{r}_\lambda, \vec{r}_\kappa) \sim \prod_{i,j,l} M_i(\vec{r}_\lambda) M_j(\vec{r}_\kappa) N_l(\vec{r}_\lambda, \vec{r}_\kappa), \tag{17}$$

where N_l, M_i are defined by Eqs. (13) and (14). The products extend over all different nearest neighbors to particles (λ, κ). Let the integrand of $M_i(\vec{r}_\lambda)$ be $I(\vec{r}_\lambda, \vec{r}_i, \vec{R}_i)$ and of $N_l(\vec{r}_\lambda, \vec{r}_\kappa)$, $H(\vec{r}_\lambda, \vec{r}_\kappa, \vec{r}_i, \vec{R}_i)$. A Monte Carlo integration routine is used to evaluate these integrals, in which case they are expressed as sums:

$$G(\vec{r}_\lambda, \vec{r}_\kappa) \sim \prod_{i,j,l} \left(N^{-1} \sum_{n=1}^{N} I_n(\vec{r}_\lambda, \vec{r}_{in}, \vec{R}_i) \right)_i \left(N^{-1} \sum_{n=1}^{N} I_n(\vec{r}_\kappa, \vec{r}_{jn}, \vec{R}_j) \right)_j \left(N^{-1} \sum_{n=1}^{N} H_n(\vec{r}_\lambda, \vec{r}_\kappa, \vec{r}_{ln}, \vec{R}_l) \right)_l . \tag{18}$$

In a bcc lattice structure and with (λ, κ) nearest neighbors, there are 14 such three-dimensional integrals (sums). The index n on the set of vectors $\Pi_{i,j,l}\{\vec{r}_{in}, \vec{r}_{jn}, \vec{r}_{ln}\}$ specifies a particular value for these 14 vectors, selected at random. Each three-dimensional integral in Eq. (18) is evaluated by summing the N values of its integrand, obtained using the N randomly selected vectors $\{\vec{r}_{in}\}$, and then dividing by N. It is important to note that the integral $M_i(\vec{r}_\lambda)$ with integrand $I(\vec{r}_\lambda, \vec{r}_i, \vec{R}_i)$ and $M_j(\vec{r}_\lambda)$ with integrand $I(\vec{r}_n, \vec{r}_j, \vec{R}_j)$, $i \neq j$, are independent of one another with respect to the vari-

ables $\vec{r}_i$ and $\vec{r}_j$. Clearly, every integral in $G(\vec{r}_\lambda, \vec{r}_\kappa)$ is independent of one another in the set of variables $\Pi_{i,j,l}\{\vec{r}_i, \vec{r}_j, \vec{r}_l\}$. This means that the same randomly selected vector, $\vec{a}_n$, which is used to evaluate one integrand at one point, may also be used to evaluate the integrands in all the sums of Eq. (18).

Hence, instead of selecting 3×14 different random values to define the vectors in the set $\Pi_{i,j,l}\{\vec{r}_{in}, \vec{r}_{jn}, \vec{r}_{ln}\}$, at one point in phase space, a single vector $\vec{a}_n$ can be used to evaluate the integrand in each of the 14 sums. This, of course,

TABLE VI. Product of correlation functions approximation. Energy calculated from the dynamic-field approximation incorporating pair correlations between particles (λ, κ) and their first; first and second; or first, second, and third shells of nearest neighbors.

Number of $f(r_{ij})$ products in calculation of $G(\vec{r}_\lambda, \vec{r}_\kappa)$	$\langle V \rangle$ (K)	$\langle T \rangle$ (K)	$\langle E_0 \rangle$ (K)
1st-nearest neighbors	−24.10	20.40	−3.70
1st- and 2nd-nearest neighbors	−25.17	19.95	−5.22
1st-, 2nd-, and 3rd-nearest neighbors	−25.10	19.95	−5.15

TABLES VII. Energy contribution from different nearest-neighbor shells in lattice sum.

Volume (cm³/mole)	Nearest-neighbor shell	Contribution to ⟨V⟩ (K) Dynamic field	Rigid lattice	Contribution to ⟨T⟩ (K) Dynamic field	Rigid lattice	Contribution to E_0 (K) Dynamic field	Rigid lattice
21.60	1st	−14.95		12.50		−2.45	
	2nd	−6.64		2.38		−4.26	
	3rd–10th	−5.33		0.97		−4.36	
	11th–38th	−0.39	−0.39	0.03	0.03	−0.36	−0.36
				6.25	$= 3\hbar^2\beta/4m$	+6.25	
	Total	−27.31		22.13		−5.18	
10.25	1st	+8.77		42.45		51.22	
	2nd	−11.45		8.92		−2.53	
	3rd	−8.19		1.84		−6.35	
	4th	−5.52	−5.69	1.03	1.00	−4.49	−4.69
	5th–10th	−4.93	−4.96	0.70	0.70	−4.23	−4.26
	11th–38th	−1.74	−1.74	0.15	0.15	−1.59	−1.59
				27.80	$= 3\hbar^2\beta/4m$	+27.80	
	Total	−23.06		82.89		59.83	

simplifies the evaluation considerably. $G(\vec{r}_\lambda, \vec{r}_\kappa)$ is then substituted into Eq. (8) and the resulting six-dimensional integral is solved to obtain the energy.

As an experiment, it was decided to constrain the motion of the atoms comprising the molecular field in such a way that they all move in concert about (λ, κ) as a single entity. That is, the displacement vectors of all nearest-neighbor molecular-field atoms are taken to be the same, $(\vec{y}_n = \vec{r}_{in} - \vec{R}_i,\ i = 1, 2, \ldots, 14)$, in each configuration used in evaluating $G(\vec{r}_\lambda, \vec{r}_\kappa)$. The $\vec{y}_n$ are selected randomly to generate other configurations. Then, Eq. (18) becomes

$$G(\vec{r}_\lambda, \vec{r}_\kappa) \sim N^{-1} \sum_{n=1}^{N} \left(\prod_{i,j,l} I_{ni}(\vec{r}_\lambda, \vec{y}_n, \vec{R}_i) I_{nj}(\vec{r}_\kappa, \vec{y}_n, \vec{R}_j) H_{nl}(\vec{r}_\lambda, \vec{r}_\kappa, \vec{y}_n, \vec{R}_l) \right). \tag{19}$$

The value of the energy, obtained with $G(\vec{r}_\lambda, \vec{r}_\kappa)$ calculated in this fashion, agrees to within 1% of the exact numerical evaluation. Within the statistical error associated with the Monte Carlo

FIG. 15. Comparison of $R(r)$ and $e^{-\beta r^2}$ for solid ^{4}He at two different volumes.

integration routine, the results of these two different methods of calculation agree completely. This conclusion was fortified by comparing results of the two methods at several different volumes for ^{3}He and ^{4}He. As a result, the calculation of $G(\vec{r}_\lambda, \vec{r}_\kappa)$, as expressed by Eq. (19), requires the solution of only one three-dimensional integral rather than 14 such integrals. The total energy then results from the evaluation of a nine-dimensional integral. The considerable simplification of algebraic analysis is obvious.

Although we do not fully understand all the implications of this result, it does seem apparent that the dynamical behavior of an arbitrary pair (λ, κ) is insensitive to the relative orientations of the molecular-field atoms with respect to one another but instead depends only on their individual orientations with respect to (λ, κ). In practice the evaluation of Eq. (8) utilized the following procedure. All of the equations were first rewritten for the computer program in terms of the vector displacement of each molecule from its equilibrium lattice site. That is, the following vectors were introduced:
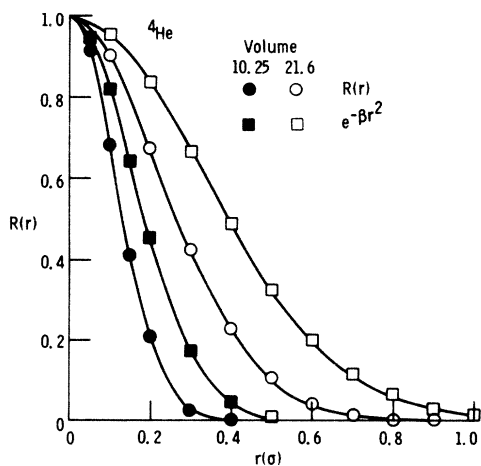
$$\vec{r} \equiv \vec{r}_\kappa - \vec{R}_\kappa, \quad \vec{z} \equiv \vec{r}_\lambda - \vec{R}_\lambda,$$

$$\vec{Y} \equiv \vec{r}_s - \vec{R}_s = \vec{r}_\rho - \vec{R}_\rho. \tag{20}$$

Six random numbers were chosen for the components of the $\vec{r}$ and $\vec{z}$ vectors. Importance sampling was used for the two random numbers chosen for $|\vec{r}|$ and $|\vec{z}|$. It was found that biasing the other four variables had a much smaller effect on statis-

tics and was therefore not employed. For this six-dimensional point in phase space $G(\vec{r}_\lambda \ \vec{r}_\kappa)$ was evaluated using one of the above techniques. This process was repeated for a total of typically 10 000 to 100 000 points. It is estimated that the computer time used was approximately an order of magnitude less than for a full Monte Carlo simulation for comparable statistical errors.

---

[1]J. P. Hansen and D. Levesque, Phys. Rev. 165, 293 (1968).

[2]J. P. Hansen and E. L. Pollock, Phys. Rev. A 5, 2651 (1972).

[3]T. A. Bruce, Phys. Rev. B 5, 4170 (1972).

[4]W. W. Wood and F. R. Parker, J. Chem. Phys. 27, 720 (1957); W. W. Wood, Physics of Simple Liquids (North-Holland, Amsterdam, 1968).

[5]R. D. Etters, J. C. Raich, and C. Cochran, J. Low Temp. Phys. 9, 53 (1972); L. W. Bruch and I. J. McGee, J. Chem. Phys. 46, 2959 (1967).

[6]J. P. Hansen, Phys. Lett. A 34, 25 (1971).

[7]J. de Boer and A. Michiels, Physica (Utr.) 5, 945 (1938).

[8]A. M. Michels, W. deGraff, and C. A. tenSeldam, Physica (Utr.) 26, 393 (1960).

[9]L. H. Nosanow, Phys. Rev. 98, 1479 (1955).

[10]R. A. Guyer, Solid State Commun. 7, 315 (1969).

[11]R. D. Etters, J. C. Raich, and R. L. Danilowicz, Nuovo Cimento Lett. 4, 667 (1970).

[12]D. O. Edwards and R. C. Pandorf, Phys. Rev. 140, 816 (1965); Phys. Rev. 169, 222 (1968).

[13]A. K. McMahan, J. Low Temp. Phys. 18, 159 (1972).

[14]H. Horner, Phys. Rev. A 1, 1712 (1970); Phys. Rev. A 1, 1719 (1970).

[15]R. D. Etters, J. C. Raich, and Prakash Chand, J. Low Temp. Phys. 5, 711 (1971).

[16]E. L. Pollock, T. A. Bruce, G. V. Chester, and J. A. Krumhansl, Phys. Rev. B 5, 4180 (1972).

[17]J. W. Stewart, J. Phys. Chem. Solids 1, 146 (1956).

[18]C. A. Swenson (private communication).